

# Phased Array Combined with 3D-printed Dielectric Lens for Millimeter Wave Fixed Wireless Access

T. Q. K. Nguyen<sup>1</sup>, F. Ferrero<sup>2</sup>, T. Q. V. Hoang<sup>1</sup>, E. Vandelle<sup>1</sup>, S. Wane<sup>3</sup>, P. Ratajczak<sup>4</sup>, D. Slock<sup>5</sup>

<sup>1</sup>*Thales Research & Technology, Palaiseau, France*

<sup>2</sup>*Laboratoire LEAT, Université Côte d'Azur, Sophia Antipolis, France*

<sup>3</sup>*EV-Technologie, Caen, France*

<sup>4</sup>*Orange Lab, Sophia Antipolis, France*

<sup>5</sup>*EURECOM, Sophia Antipolis, France*

tran-quang-khai.nguyen@thalesgroup.com

**Abstract**—In order to provide an energy-efficient link for 5G millimeter-wave Fixed Wireless Access (FWA), a planar dielectric multifocal lens antenna architecture is investigated. A scan range of  $\pm 30^\circ$  is targeted to ensure better angle-of-arrival correction. In addition, modulation of the radiating elements is explored to improve scanning resolution and reduce spillover loss for a planar lens solution coupled to a small antenna array. These elements are first evaluated using a semi-analytical approximation, paving the way for future rapid optimization. Preliminary numerical and experimental evaluations demonstrate that the approximation is sufficiently precise and the lens-based phased array concept is flexible and advantageous in terms of energy efficiency compared to the conventional phased array approach.

**Index Terms**—beam steering, EIRP, phased array, planar lens, spillover.

## I. INTRODUCTION

In recent years, the development of antenna technology has been crucial in meeting the demands of emerging high-frequency applications, particularly within the 5G millimeter-wave (mmW) bands. Taking advantage of advanced 5G+ technologies like beam-forming at millimeter wave frequencies, FWA delivers broadband services to locations without traditional wired infrastructure [1]. Essential for FWA to be functional is a very high level of Effective Isotropic Radiated Power (EIRP). This can be achieved by high directivity antennas installed on exterior walls of individual homes or professional buildings [2]. Beam steering across an small angular scanning range is crucial for mitigating misalignment during device installation or displacement caused by factors such as wind, vibrations, or temperature fluctuations. Moreover, these antennas must prioritize energy efficiency and be capable of supporting multiple frequency bands and multibeams to meet diverse service requirements as stipulated by the International Telecommunication Union (ITU).

Quasi-optical systems, based on dielectric lens coupled to a small planar antenna array, are well known for highly directive radiation pattern, overcoming the attenuation problems inherent in mmW transmission. Integrated lens antenna (ILA) solution is often adopted with lens's aperture much larger than the radiating element, offering a scanning up to  $\pm 40^\circ$ . Nevertheless, an ILA suffers from mismatch from nearfield reflections and is usually bulky.

Scan loss comes mostly from the displacement of the feed from the focal arc [3]. When required scanning range is reduced, such as  $\pm 30^\circ$  or below, a planar diffractive sub-wavelength structure can be deployed. This solution is not only more compact, but also offers improved gain and a large bandwidth [4], [5]. Likewise, different scan loss enhancement techniques can be applied directly on planar lens design, by use of multifocal principle [6] or by offset unifocal phase symmetry [7].

Many extensive studies from channel model point of view have also been done to tackle different limitations of lens antenna array and improve the spectral efficiency. Conventional switching lens antenna has sparse beams due to discrete feeding. This can be addressed by amplitude modulation on multiple feeds [8]. Even for an array with larger than  $\lambda_0/2$  inter-element spacing, a more sophisticated optimization of feeding can be applied to optimize null-filling and scanning range [9]. In [10], the authors discuss and propose a beam aligning precoding method to address the leakage problem due to the sparse array element's positions. [11], [12] propose working on sub-array lens system instead of single lens array, the power consumption is estimated up to 194% more efficient with a slightly compromised data rate in comparison to conventional hybrid multiple input multiple output (MIMO) architecture. Interestingly, the single-lens architecture being less complex also has its energy efficiency improved up to 150%.

This paper investigates the design considerations and validations of using a small antenna array coupled with a planar multifocal 3D-printed lens to achieve superior control over the radiation pattern in 5G mmW bands. Simulations and practical results are discussed highlighting the potential of this configuration in enhancing the scan loss performance with higher scanning resolution. This approach not only paves the way for more efficient and powerful antenna designs but also opens up new possibilities for compact and high-performance antenna systems in demanding 5G applications, especially FWA.

## II. BEAMFORMER AND COLLIMATION STRUCTURE

This joint study is supported by Energy Efficient Millimeter Wave for Fixed Wireless Access (EEMW4FIX) collaborative project [13]. The co-integration of the collimating structure with a phase array for point-to-point communication is investigated and the different partners are covering the different blocks needed for the system as shown in Fig. 1. EV-Technologies is providing a beamforming circuit for FR2 bands (26-30 GHz) with 8 channels. The circuit is using SMPM connector to feed an 1x8-element-array whose inter-element spacing is 5 mm, corresponding to a half-wavelength at 30 GHz.

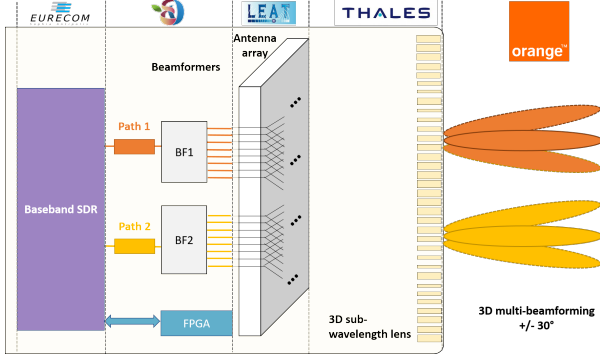


Fig. 1. Beamformer and collimation structure concept.

The phase and amplitude of the beamformer's channels are controlled with 6 bits ( $5.625^\circ$  resolution) and 5 bits (0.5 dB step), respectively. The beamformer also integrates power amplifier and low-noise amplifier for Tx/Rx operation [14], [15]. The power consumption depends on the number of activated outputs. In transmit mode, it typically varies from 1 W for 1 output to 4 W for 8 outputs with 18 dBm saturated power per channel. As shown in Fig. 1, one or multiple phase arrays can be integrated to provide multibeam capabilities.

### A. Lens-based phased array concept

The combination of a beamformer circuit and a collimating structure can provide the following advantages:

- Any of the 8 output channels of the beamformer can be activated to create a beam in a different direction.
- 2 neighbored elements of the antenna array can be activated at the same time to generate an intermediate beam direction. Moreover, by tuning the amplitude of these elements, the phase center is virtually shifted and a continuous scanning range (between directions generated by these elements separately) can be achieved.
- A phase shift between two elements can be used to reduce the spillover in large scanning.

In this work, we propose an architecture fully integrated. An array of antennas is connected to a beamformer circuit allowing the generation of complex power coefficients feeding to each element. The coefficient vector normally contains only an activated sub-array with or without a phase difference. A progressive phase difference can be applied to further optimize

the spillover energy under the lens, the effect will be discussed in the next section. The rest of the array is switched off to reduce the power consumption. The sub-array is coupled to a planar multifocal sub-wavelength lens. The angular beam-scanning performance is due to the discrete spatial position of the array's element positions with respect to the center of the lens in the focal plane. The finer angular resolution is obtained by tuning the amplitude of the elements. Multibeam performance and null control can also be implemented with this architecture.

### B. Multifocal lens design

The conventional unifocal lens is thoroughly studied in the literature. In this study, a lens is placed in  $Oxy$  plane. Given a point source positioning at  $(dx, dy)$  and at the focal distance  $F$  to the lens, to compensate the arriving phase and convert the spherical to plane wave so that the output wave beams to  $(\theta, \phi)$  direction, representing by vector wavenumber  $\mathbf{k}_0$ , the phase profile function of the unifocal lens is:

$$\Phi^{unif} = \mathbf{k}_0 \cdot (\hat{x} + \hat{y}) - k_0 \sqrt{(x - dx)^2 + (y - dy)^2 + F^2} \quad (1)$$

where  $k_0$  is the absolute wavenumber. The unifocal lens phase profile is hence a function of  $(\theta, \phi, dx, dy)$ . If the radiation of the source is known and highly polarized, the unifocal lens's phase profile can also be calculated as follows:

$$\Phi^{unif} = \mathbf{k}_0 \cdot (\hat{x} + \hat{y}) - \angle \mathbf{E}_{in} \quad (2)$$

where  $\mathbf{E}_{in}$  is the dominant component of the known E-field at the input plane of the lens and operator  $\angle \mathbf{A}$  gives the angle matrix of complex matrix  $\mathbf{A}$ . This adaptation gives a better collimation for the  $\mathbf{k}_0$  direction.

It should be noted that the focal points of a unifocal lens are on a semi-circle focal arc [3]. Therefore, while a unifocal lens defined by (1) or (2) collimates very well for the  $\mathbf{k}_0$  direction, displacing the source in the plane parallel to the lens makes it off-focal and susceptible to scan loss, especially for high directivity lens.

The effectiveness of multifocal lens design in overcoming the scan loss limit has been widely discussed in the literature. The analytical calculation of the lens phase profile is proposed as weighted average  $N$  unifocal corrections as follows:

$$\Phi^{multif} = \frac{\sum_{i=1}^N \mathbf{A}_i \cdot \Phi_i^{unif}}{\sum_{i=1}^N \mathbf{A}_i} \quad (3)$$

where the superscript  $i$  enumerates the  $i^{th}$  focal and  $N$  is the number of unifocal corrections. The Gaussian coefficient matrices are defined as:

$$\mathbf{A}_i = \exp\left(-\frac{(x - dx_i)^2 + (y - dy_i)^2}{2\sigma_i^2}\right) \quad (4)$$

and the corresponding unifocal profile matrix  $\Phi_i^{unif}$  is calculated at  $(dx_i, dy_i)$  and for direction  $\mathbf{k}_{0i}$ . The N-focal lens phase profile is hence defined by inputs:

$$\Phi^{multif} \left( \begin{array}{c} (\theta_1, \phi_1, dx_1, dy_1) \\ \dots \\ (\theta_N, \phi_N, dx_N, dy_N) \end{array} \right) \quad (5)$$

For the sake of simplicity,  $\sigma$  is set equal to the focal distance  $F$  in calculations in the next section.

### III. SEMI-ANALYTICAL MODEL AND VALIDATION

#### A. Semi-analytical model

Lens antenna design is well known for very long procedures if using pure numerical simulations because of the large size with respect to wavelength and the high complexity of the lens structure. We propose the below simplified semi-analytical calculation with numerical input, allowing reducing significant the optimization time.

The planar structure of a thin lens allows simplifying the analysis of the structure. Lossless lens operation can be modeled as a dot product of the E-field input  $\mathbf{E}_{in}$  and the lens's phase profile  $\Phi$ :

$$\mathbf{E}_{out} = \mathbf{E}_{in} \cdot e^{j\Phi} \quad (6)$$

The analysis is proceeded by expanding the spatial E-field onto the spectral basis  $\mathcal{E}$  by Fourier transform [16]:

$$\mathcal{E}_{out}(k_x, k_y, z) = \int_{-\infty}^{\infty} \int_{-\infty}^{\infty} \mathbf{E}_{out} e^{-j\mathbf{k}\cdot\mathbf{r}} dx dy \quad (7)$$

where  $\mathbf{k}$  denotes the spectral variable and  $\mathbf{r}$  denotes the transversal position to the center of the lens. The inverse operation, done by another Fourier transform, allows evaluating the source translation or propagation in the spatial domain, as in Fig. 3:

$$\mathbf{E}_{out}(x, y, z) = \frac{1}{4\pi^2} \int_{-\infty}^{\infty} \int_{-\infty}^{\infty} \mathcal{E}_{out} e^{j\mathbf{k}\cdot\mathbf{r}} dk_x dk_y \quad (8)$$

The fact that  $\mathbf{E}_{in}$  can be either analytical, numerical or even experimental data makes this approximation very flexible and computationally efficient.

Certain behaviors of the lens and source configuration can be observed by the semi-analytical approximation. For example in Fig. 2, the scan loss performance of either a single Hertzian dipole [17] or an equal-phase array of  $1 \times 2$  y-polar Hertzian dipoles along x-axis under either a large unifocal or a large bifocal lens is studied. In other to avoid the spillover, the aperture of the lenses are designed to be sufficiently large. Precisely, the lenses' diameter is around  $36\lambda_0$ , placing at  $F \approx 7.2\lambda_0$ , so  $F/D \approx 0.2$ . The unifocal lens is designed to collimate the wave front from a point source placing at the center, this leads to a very high directivity for normal angle. On the other hand, because of aberrations, the scan loss is extremely bad at high oblique angles, i.e. -6 dB at  $30^\circ$ . An array radiation as illumination source makes the directivity slightly lower at normal angle due to the aperture efficiency while improving the scan loss. The improvement in terms of scan loss is much clearer in the case of bifocal lens between

single and array source. The array of  $1 \times 2$  Hertzian dipoles has higher gain at all angles of incident in comparison to a single Hertzian dipole. Interestingly, the result implies that dual sources should be prioritized upon scan loss optimization.

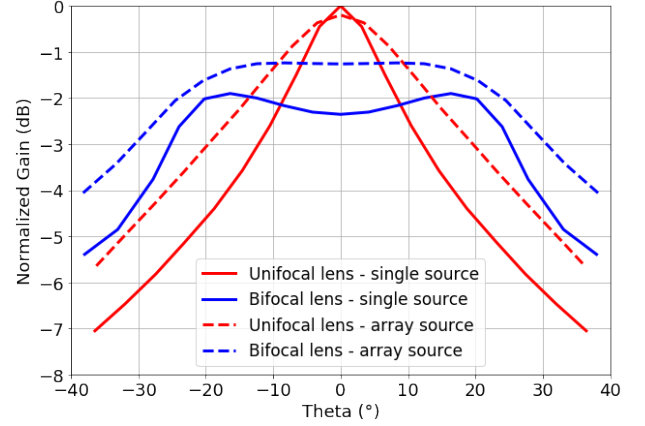


Fig. 2. Scan loss performance of single element (solid line) and  $1 \times 2$  Hertzian dipole array (dashed line) illuminating either a unifocal (red line) or bifocal (blue line) lens.

In another example, we study the effects of the finite aperture of the planar lens. In this case, the displacement of the source causes spillover, especially in case of big position offset and/or a large radiation beamwidth. Using a small array of  $1 \times 2$  y-polar Hertzian dipoles source concentrates the illumination under the lens. Furthermore, a modulation of phase and amplitude can also direct the illumination zone toward the centre of the lens for even lower leakage, as illustrated in Fig. 3. The same utility has been illustrated in [18] to avoid high reflection at a volumetric lens. In Fig. 4, a small improvement (about 0.4 dB) at the main beam can be observed together with reduced side lobes at  $20^\circ - 40^\circ$  thanks to the phase shift applied to a  $1 \times 2$  array source placed at  $+4.5\lambda_0$  offset in x-axis.

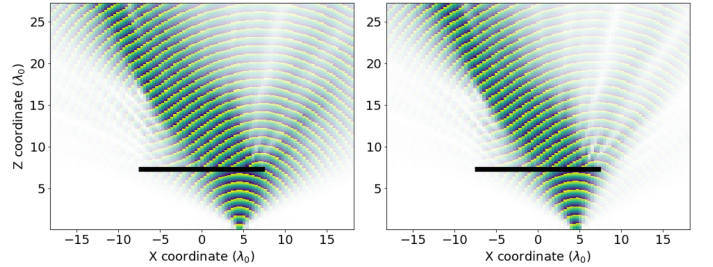


Fig. 3. Spillover leakage from a wide beam single element source illuminating a lens (left) is reduced by beam forming under the lens using a  $1 \times 2$  array (right). Lens aperture is represented by black lines.

The analysis above prepares a framework for a fast evaluation and optimization of the entire system in the future development steps. These observations help define in advance the configuration of the lens and the specifications for the antenna array. Preliminary numerical and experimental validations of the design are discussed in the next sub-sections.

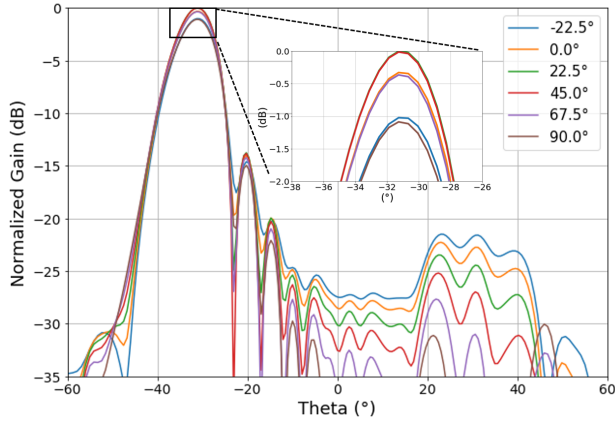


Fig. 4. Spillover reduction thanks to phase modulation of  $1 \times 2$  array source.

### B. Numerical validation

To validate the semi-analytical model and the advantage of multifocal lens compared to unifocal lens, two designs have been generated to be combined with a patch array: a unifocal lens defined by:

$$\Phi^{unif}(0^\circ, 0^\circ, 0, 0)$$

and a bifocal lens defined by:

$$\Phi^{bif} \left( \begin{matrix} (-15^\circ, 0^\circ, +2\lambda_0, 0) \\ (+15^\circ, 0^\circ, -2\lambda_0, 0) \end{matrix} \right)$$

The lenses have the same aperture of 160 mm and focal distance of 60 mm, leading to an  $F/D = 0.375$ .

The computed phase profiles are synthesized by using sub-wavelength circular pillars with different diameters in the composite material with high permittivity and low loss ( $\epsilon_r = 7.5$ ,  $\tan\delta = 0.001$ ) [19]. By spatially varying the pillar diameter, any desired phase profile can be synthesized. This method has been detailed in our previous work [4], [20]. Once the lenses' geometries are generated, full-wave simulations are performed using the Transient Solver of CST Microwave Studio 2022. Fig. 5 illustrates the simulation configuration of an array of patches combined with the unifocal lens.

Fig. 6 compares the radiation patterns calculated from the approximation presented above and from the full-wave simulation with CST. It should be noted that the input of the semi-analytical model is the E-field at the focal distance exported from a full-wave simulation of the  $2 \times 2$  patch array. The  $0^\circ$  and  $15^\circ$  beams correspond to 0 mm and 21.7 mm (corresponding to  $2\lambda_0$  at 27.25 GHz) displacements of the source, respectively, with respect to the lens center. A very good agreement is observed for the main beam direction and the main beam width, allowing the validation of the proposed model. The difference in radiation levels at high angles is due to the finite size of the integral operations and the thickness of the lens. These constraints can be further addressed if higher precision is required, with a costlier computation.

As expected, when compared to the unifocal lens, the bifocal one slightly degrades the performance at  $0^\circ$  (about

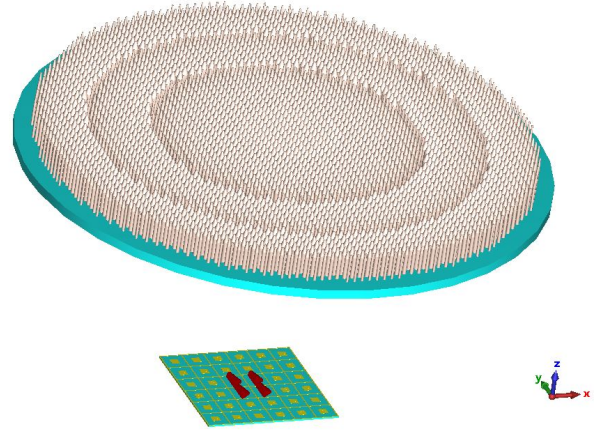


Fig. 5. Simulation configuration in CST of an array of patches coupled to the unifocal dielectric lens.

0.3 dB drop) but improves the performance when scanning (about 0.6 dB better at  $15^\circ$ ). Converting to scan loss value at  $15^\circ$ , the bifocal lens presents 0.5 dB versus 1.3 dB with the unifocal lens. These results confirm the advantage of using a bifocal lens for beam scanning. One can note that this enhancement would be more significant for higher scanning angles.

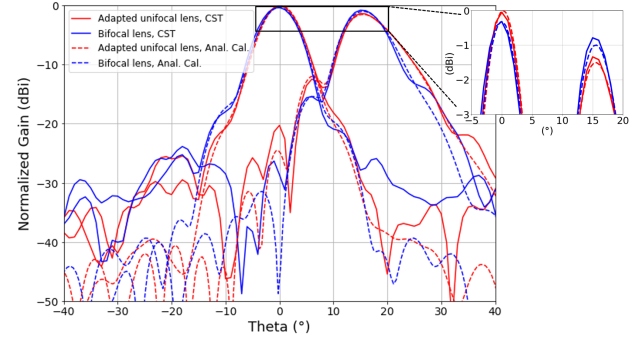


Fig. 6. Radiation patterns of unifocal lens (red line) and bifocal lens (blue line) from numerical simulation (solid line) and semi-analytical approximation (dashed line) for beam-scanning at  $0^\circ$  and  $15^\circ$ .

Moreover, it is worth highlighting that the approximation only takes a few minutes, whereas a full numerical simulation combining the antenna array with the dielectric lens takes up to several hours even by powerful computers.

### C. Preliminary experimental validation

The aforementioned unifocal lens is fabricated in a single-step 3D-printing process with the advanced FDM technique presented in [21]. The compact range measurement system ATS800 is used to assess the structure performance as shown in Fig. 7.

The 16 cm-diameter lens is placed at a distance of 60 mm from the antenna array. The antenna array is shifted by 38 mm with respect to the center of the lens. In this configuration and by activating the two radiating elements at the center of

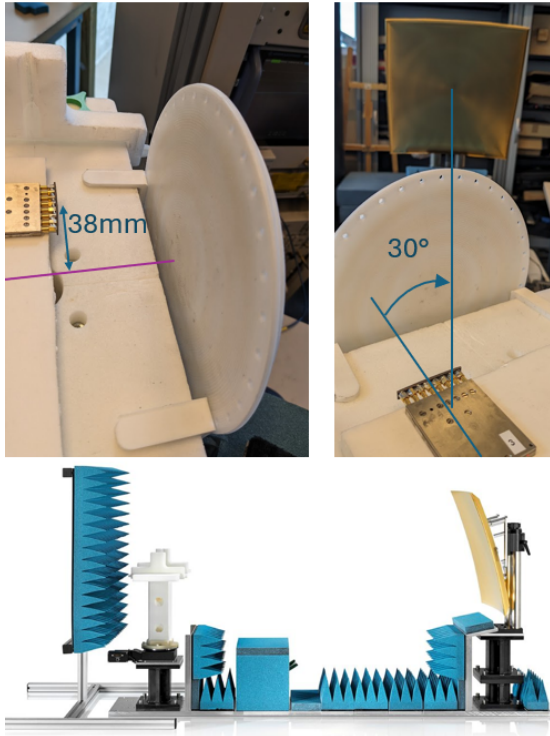


Fig. 7. AT800 measurement set-up for beam-scanning at  $30^\circ$

the array, the main beam steers at  $30^\circ$ . The whole system (lens combined to antenna array) is then rotated by  $30^\circ$  to focus the beam toward the reflector of the compact range. The phase shift between the two elements is swept from  $-22.5^\circ$  to  $90^\circ$  and the total transmission level is measured. Thanks to a proper illumination of the sub-array, obtained with  $45^\circ$ -phase-shift, toward the lens, the transmission level is increased by 0.37 dB as shown in Table I. Interestingly, similar performance is observed in Fig 4 when analytically calculating the system of  $1 \times 2$  Hertzian dipole array coupled to a unifocal lens. These preliminary results validate the advantage of applying phase shift to the elements in the sub-array to reduce the spillover loss, thus improve the aperture efficiency.

TABLE I  
USING PHASE SHIFT FOR SPILLOVER REDUCTION

Phase shift	Maximum normalized transmission level (dB)
$-22.5^\circ$	-0.80
$0^\circ$	-0.37
$22.5^\circ$	-0.06
$45^\circ$	0
$67.5^\circ$	-0.31
$90^\circ$	-0.64

#### IV. CONCLUSION

In this work, we present an architecture of lens antenna integrating a beamformer circuit. A semi-analytical approximation has been adopted, allowing quick evaluation of different parameters of the lens design and source configuration before

validating in numerical simulation. Preliminary measurements were also carried out, showing a good agreement to numerical simulation and confirm the power consumption efficiency for an optimal EIRP.

In future studies, we will continue to further validate the concept of multifocal lens design in measurement. The experimentally validated design with its performance will be used to evaluate the energy efficiency in a channel model.

#### ACKNOWLEDGMENT

The authors acknowledge the financial support provided by the French agency of research under the EEMW4FIX project. Special thanks to NANOE for the fabrication of the 3D-printed lens and R&S for the measurement setup.

#### REFERENCES

- [1] T. S. Rappaport et al., "Millimeter Wave Mobile Communications for 5G Cellular: It Will Work!," in *IEEE Access*, vol. 1, pp. 335-349, 2013, doi: 10.1109/ACCESS.2013.2260813.
- [2] R. Kalimulin, A. Artemenko, R. Maslennikov, J. Putkonen and J. Salmelin, "Impact of mounting structures twists and sways on point-to-point millimeter-wave backhaul links," 2015 IEEE International Conference on Communication Workshop (ICCW), London, UK, 2015, pp. 19-24, doi: 10.1109/ICCW.2015.7247069.
- [3] Y. Zeng and R. Zhang, "Millimeter Wave MIMO With Lens Antenna Array: A New Path Division Multiplexing Paradigm," in *IEEE Transactions on Communications*, vol. 64, no. 4, pp. 1557-1571, April 2016, doi: 10.1109/TCOMM.2016.2533490.
- [4] A. O. Diallo, R. Czarny, B. Loiseaux and S. Holé, "Comparison Between a Thin Lens Antenna Made of Structured Dielectric Material and Conventional Lens Antennas, in Q-Band in a Compact Volume," in *IEEE Antennas and Wireless Propagation Letters*, vol. 17, no. 2, pp. 307-310, Feb. 2018, doi: 10.1109/LAWP.2017.2787789.
- [5] R. Czarny et al., "Q-band high gain radome integrated lens antenna for compact backhaul terminal," 2017 11th European Conference on Antennas and Propagation (EUCAP), Paris, France, 2017, pp. 2771-2775, doi: 10.23919/EuCAP.2017.7928326.
- [6] S. A. Matos, E. B. Lima, J. R. Costa, C. A. Fernandes and N. J. G. Fonseca, "Design of a 40 dBi planar bifocal lens for mechanical beam steering at Ka-band," 2016 10th European Conference on Antennas and Propagation (EuCAP), Davos, Switzerland, 2016, pp. 1-4, doi: 10.1109/EuCAP.2016.7481442.
- [7] P. Mei, G. F. Pedersen and S. Zhang, "Performance Improvement of Mechanically Beam-Steerable Transmitarray Antennas by Using Offset Unifocal Phase Symmetry," in *IEEE Transactions on Antennas and Propagation*, vol. 71, no. 1, pp. 1129-1134, Jan. 2023, doi: 10.1109/TAP.2022.3218942.
- [8] A. Artemenko, A. Mozharovskiy, S. Tikhonov, A. Myskov and R. Maslennikov, "Multiple-feed integrated lens antenna with continuous scanning range," 2017 11th European Conference on Antennas and Propagation (EUCAP), Paris, France, 2017, pp. 2795-2799, doi: 10.23919/EuCAP.2017.7928857.
- [9] W. Wang, N. Estes, N. C. Garcia, M. Roddy, A. K. Bolstad and J. D. Chisum, "Beamforming Phased-Array-Fed Lenses With  $> 0.5\lambda$ -Spaced Elements," in *IEEE Transactions on Antennas and Propagation*, vol. 71, no. 3, pp. 2208-2223, March 2023, doi: 10.1109/TAP.2023.3240085.
- [10] T. Xie, L. Dai, D. W. K. Ng and C. -B. Chae, "On the Power Leakage Problem in Millimeter-Wave Massive MIMO With Lens Antenna Arrays," in *IEEE Transactions on Signal Processing*, vol. 67, no. 18, pp. 4730-4744, 15 Sept.15, 2019, doi: 10.1109/TSP.2019.2926019.
- [11] L. Afeef, G. Mumcu and H. Arslan, "Energy and Spectral-Efficient Lens Antenna Subarray Design in MmWave MIMO Systems," in *IEEE Access*, vol. 10, pp. 75176-75185, 2022, doi: 10.1109/ACCESS.2022.3190866.
- [12] M. Karabacak, H. Arslan and G. Mumcu, "Lens Antenna Subarrays in mmWave Hybrid MIMO Systems," in *IEEE Access*, vol. 8, pp. 216634-216644, 2020, doi: 10.1109/ACCESS.2020.3041633.
- [13] ANR EEMW4FIX project : <https://anr.fr/Project-ANR-21-CE24-0028>

- [14] S. Wane et al., "Broadband Smart mmWave Front-End-Modules in Advanced FD-SOI with Adaptive-Biasing and Tuning of Distributed Antenna-Arrays," 2020 IEEE Texas Symposium on Wireless and Microwave Circuits and Systems (WMCS), Waco, TX, USA, 2020, pp. 1-5, doi: 10.1109/WMCS49442.2020.9172398.
- [15] EVT-smBFN2630-1x8, accessed on the 07/05/2024 : [https://ev-technologies.com/wp-content/uploads/2023/06/2023-06-09\\_One-Page-BeamFormer-copy.pdf](https://ev-technologies.com/wp-content/uploads/2023/06/2023-06-09_One-Page-BeamFormer-copy.pdf)
- [16] P. Clemmow, "The plane wave spectrum representation of electromagnetic fields," Pergamon Press (Oxford and New York), 1966.
- [17] J. R. Wait, Electromagnetic wave theory, Harper Row, 1985.
- [18] M. A. Campo et al., "D-Band Active Antenna Array with Lens Enabling Quasi-Optical and Analogue Beam Reconfiguration for 6G Applications," 2024 18th European Conference on Antennas and Propagation (EuCAP), Glasgow, United Kingdom, 2024, pp. 1-4, doi: 10.23919/EuCAP60739.2024.10501233.
- [19] T. Q. V. Hoang et al., "Benefits of Using a High-permittivity and Low-loss Printable Material for Sub-wavelength Deflectors," 2023 IEEE Conference on Antenna Measurements and Applications (CAMA), Genoa, Italy, 2023, pp. 492-496, doi: 10.1109/CAMA57522.2023.10352874.
- [20] T. Q. V. Hoang, E. Vandelle, M. Bertrand and B. Loiseaux, "Low-Profile 2D-Mechanical-Beam-Steering Antenna with Large Field-of-View," 2024 18th European Conference on Antennas and Propagation (EuCAP), Glasgow, United Kingdom, 2024, pp. 1-5, doi: 10.23919/EuCAP60739.2024.10501310.
- [21] T. Q. V. Hoang, J. Sourice, E. Vandelle, R. Faye, M. Bertrand and B. Loiseaux, "Additive Manufacturing of a 460mm-diameter Flat Off-axis Lens for Ka-band Communications," 2023 17th European Conference on Antennas and Propagation (EuCAP), Florence, Italy, 2023, pp. 1-4, doi: 10.23919/EuCAP57121.2023.10133541.